PERGAMON

Micron 30 (1999) 235–244

micron

www.elsevier.com/locate/micron

Microfabrication techniques using focused ion beams and emergent applications

M.J. Vasile*, R. Nassar, J. Xie, H. Guo

Institute for Micromanufacturing, Louisiana Tech University, Ruston, LA 71272, USA

Received 29 September 1998; received in revised form 22 January 1999; accepted 25 January 1999

Abstract

The application of focused ion beam (FIB) machining in several technologies aimed at microstructure fabrication is presented. These emergent applications include the production of micromilling tools for machining of metals and the production of microsurgical tools. An example of the use of microsurgical manipulators in a circulatory system measurement is presented. The steps needed to transform the laboratory fabrication of these tools and manipulators into a routine FIB production process are discussed. The ion milling of three-dimensional cavities by the exact solution of a mathematical model of the FIB deflection is demonstrated. A good agreement between the model calculation and the ion beam control has been obtained for parabolic and cosine cross-section features with planes of symmetry.

Keywords: Focused ion beams; Sputter simulations; Sputter yields; Microfabrication; Micromanipulators; Microtools; Micromachining; Microsurgical tools

1. Introduction

1.1. General overview

This paper discusses new applications or potential uses of focused ion beam (FIB) techniques in microstructure fabrication. The FIB method can be either an enabling technology or the main production method. The applications discussed in this article are considered to be an emergent, i.e. outside the realm of present commercial uses of the FIB. This is not intended to be an exhaustive review of FIB technology, however the references on specific topics are recent and give the reader the path to the current state of the subject.

The FIB technology is based on field emitted ions from a liquid metal ion source (Bell and Swanson, 1985) and on the formation and deflection of high resolution ion beams from that source (Orloff, 1993). FIB have been used in numerous applications in experimental electronic and electro-optic device fabrication (Kalburge et al., 1997; Konig et al., 1998). Significant research efforts have been made to achieve ion implantation (Musil et al., 1996; Crell et al., 1997), device patterning (Gamo, 1991; Nagamchi et al., 1996) and FIB stimulated deposition of conductors and opaque films (Vasile and Harriott, 1989; Gross et al., 1990)

1.2. Commercial applications

FIB technology has evolved in directions far beyond the originally perceived application of X-ray and photomask mask repair (Blauner and Mauer, 1993). The mask repair remains a niche application at this time relative to the other uses that have been found for the technology. These uses include electron device fabrication, failure mode analysis in the integrated circuit (IC) manufacturing process (Nikawa, 1991), reverse engineering in the IC industry, step-by-step diagnostics of IC fabrication, IC test modifications, TEM sample preparation (Ishitani et al., 1998; Saka, 1998) and magnetoresisitve head trimming. The application of FIB to the formation of the pole gap in magnetoresistive heads (MRH) is the only non-diagnostic commercial use of the FIB technology to date. The production procedures using sophisticated pattern recognition programs allow considerable flexibility and accuracy in the gap (or pole shape) formation. The MRH production requires high speed machining with sub-micron accuracy and resolution, and it is a serial process.

1.3. New applications of focused ion beam milling

There is a significant potential for producing other small objects in a serial process using FIB machining. Laboratory scale exploration of FIB microfabrication has been applied to three-dimensional shapes (Ishitani et al., 1990; Young,

* Corresponding author. Fax: + 1-318-257-5104.
E-mail address: mjv@coes.latech.edu (M.J. Vasile)

0968-4328/99/$ - see front matter
PII: S0968-4328(99)00008-6

1993) and objects like scanning probe microscope tips (Vasile et al., 1991). FIB machining is well suited to a rapid alteration of the existing microdevices, and can be either one critical single step in a more complex production process (as in the MRH application) or it can be the dominant process in a relatively simple production process. The first part of this paper explores the possibilities for the production of microtool bits for machining applications and microsurgical tools by FIB in modified serial processes. The application of the FIB manufactured tools in each of these cases has been successfully demonstrated, and the probability for use of such devices beyond proof of concept experiments is high, especially in the case of micromachine tools.

The production of microstructures by a high volume, batch processes is perceived to be the most economical and reproducible method. A high volume production method for microstructures is possible with molds fabricated by FIB machining. A three-dimensional control of the ion milling will be required in most mold-forming applications, e.g. as in molds for micro-optical lenses or other small-scale optical components. The FIB ion milling in such an application must be controlled to produce a cavity with a specific geometry in a material that will serve as a mold or as a master die in a hot pressing process. The embossing master has its origin as a cavity in the FIB milling process. The positive master is plated and released from the cavity in a manner similar to the production of embossing masters in the LIGA or the deep X-ray lithography process. The fundamental difference is that the FIB process has the potential to readily produce a mold with true three-dimensional shapes.

Control of the ion milling in three dimensions with the required accuracy and resolution is the challenge (Itoh et al., 1990; Ximen et al., 1990). Our approach to this problem uses a mathematical model of the FIB sputtering process, which yields a variable ion milling time in a deflection pattern for the pre-specified geometry. Solutions obtained by the model depend strongly on the size of the pixel in the deflection control scheme vs. the ion beam dimensions, and also on the absolute sputter yields for the material and incident ion. These sputter yields must also be known as a function of the ion angle of incidence. The latter are the critical variables for ion milling a feature in three dimensions (such as a parabolic cavity) in addition to the mathematical methods used to obtain dwell times for the deflection. The technique under development in this laboratory uses the following scheme: (1) a particular ion milling geometric shape with specified depth is called for in a model routine; (2) the material, ion beam dimension, energy and current are the input data; (3) the model solves for a pixel-by-pixel dwell-time array for the ion beam and passes this array to the control microprocessor; (4) the ion beam is then vector scanned through the deflection pattern for the dwell times in the array; and (5) the process is repeated if the ion milling procedure to the final geometry is broken down into several iterations.

The following sections describe the use of the FIB process to make microtools for ultra-precision machining applications; a variation of that process to make tools for microsurgical applications, and the three-dimensional ion milling that will be needed to make embossing masters or molds. The microtool fabrication process is an example of the FIB technique as an enabling technology. The microsurgical tools or manipulators are FIB end products, in a serial production process. The three-dimensional control of ion milling for mold or master fabrication is the least well-developed of the applications treated in this article, but significant progress has been made recently, and these results will be given. These results are of interest in their own right as ion beam–solid interaction studies, as a large part of the process relies on the use of accurate absolute sputter yields.

The FIB apparatus used in this work was constructed at AT&T Bell Labs, and is described in detail in the literature. (Harriott, 1987) The ion milling is done with 20 keV Ga^+ ions field emitted from a liquid metal ion source, focused with a single three-element lens and deflected with the octapole rods, using a vector scan. The beam current is 2 nA with a spot size of 0.45 μm diameter full-width at half maximum (FWHM, Gauss distribution). The stage motion is 35 cm in *X* and 25 cm in *Y*, with an accuracy of 1 μm and a precision of 0.26 μm. Rotation of the substrates is done with an in-vacuum stepper motor through 40:1 reduction gears, giving 0.37°/pulse rotational resolution (Vasile et al., 1994).

2. Microtools for ultraprecision machining

Modern air-bearing spindle machines equipped with high precision work tables are capable of machining to submicron precision by the conventional material removal processes. The ultimate feature size that can be machined with such devices is limited by the diameter of the rotating cutting tool and the relationship between the forces generated by this tool and the strength of the material. Previous work in this laboratory utilized FIB milling to produce nominal 25 μm diameter tool bits for an ultra-precision machining center, and the proof of concept experiments showed that complex curvilinear features with free-standing walls as thin as 8 μm could be machined in polymethyl methacrylate (PMMA) (Friedrich and Vasile, 1996; Vasile et al., 1996; Friedrich et al., 1997). Tool fabrication for this work is a combination of diamond machining and FIB milling. The tool blank is tapered to a smooth 25 μm diameter cylinder in a diamond turning operation, and then facets are ion milled on the cylindrical surface, yielding extremely sharp cutting edges.

The apparatus necessary to produce these tools is a specially designed tool carrier which allows rotation of the tool blank through 360° by an in-vacuum stepper motor (Vasile et al., 1994). The number of facets and their

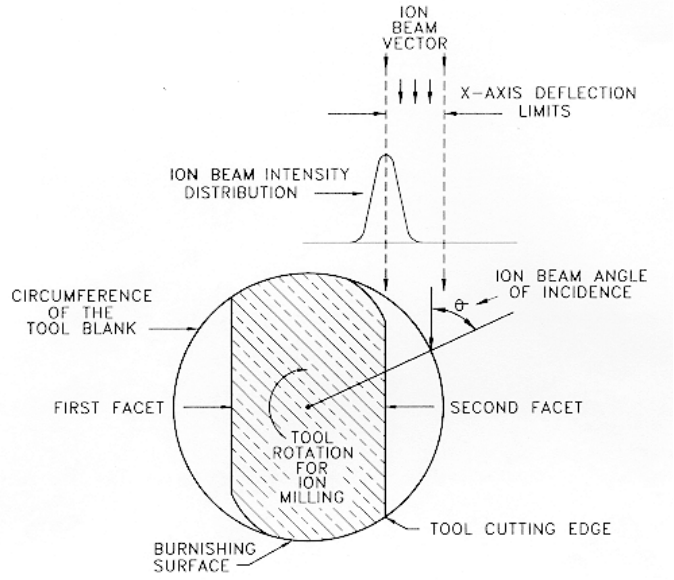

Fig. 1. End view of the ion milling process used to make a two-faceted cutting tool. The ion beam deflection limits in the *X* direction are indicated and the ''edge effect'' of the spill-over from the ion beam intensity distribution is shown. The net effect is one sharp cutting edge and one rounded edge per facet. Typical tool diameter is 25 μm, and tools with up to six facets have been made and tested.

position on the tool and the amount of burnishing surface on the circumference of the tool is controlled by the amount of rotation of the tool blank and the chord subtended by the milling depth. A diagram showing the end view of the tool cross-section and the orientation of the ion beam is shown in Fig. 1. The dimensions of the ion milling deflection field and the ion beam distribution are also indicated in Fig. 1.

A perspective view of the tool facet milling process is also shown in Friedrich and Vasile, 1996. Ion milling a facet on the tool blank must be done in a sequence that leaves sharp cutting edges on diametrically opposite sides of the tool, and the tool has burnishing surfaces left on it as indicated in Fig. 1. These cutting edges must be ion milled on the tool blank with respect to the direction of rotation intended for the tool. A multi-faceted tool with no burnishing surfaces such as the five-cutting edge 'hex tool' (Fig. 3 in Vasile et al., 1998) can be rotated in either sense, and is named a bi-directional tool. The key factors to successful tool making by FIB techniques are the smoothness of the cylindrical surface of the tool blank and the facet cutting sequence. The sharpness of the cutting edge is shown in Fig. 2, for a two-faceted tool.

The radius of curvature at the intersection of the facet surface with the cylindrical surface of the tool is less than 0.2 μm. The sharpness of this edge is simply a result of the method used in cutting the facet. The rounding effect at a feature boundary due to one-half the Gauss distribution of the ion beam is eliminated at this intersection as that portion of the ion beam is always intercepted on the top side of the tool surface as indicated in Fig. 1. The efficiency of cutting the facet is also dependent on the sputter yield as the incident angle of the ion beam with the tool surface changes. An examination of Fig. 1 shows that the angle of incidence of the ion beam with the tool surface ranges from about 45° to normal incidence. (The convention is to reference the ion beam angle of incidence to the surface normal.) The sputter yield passes through its maximum value as the facet develops, and this function has a pronounced maximum at 77° as shown for 20 keV Ga^+ on iron, in Fig. 3.

The production rate and the sharpness of the cutting edges can be optimized by taking advantage of the function shown

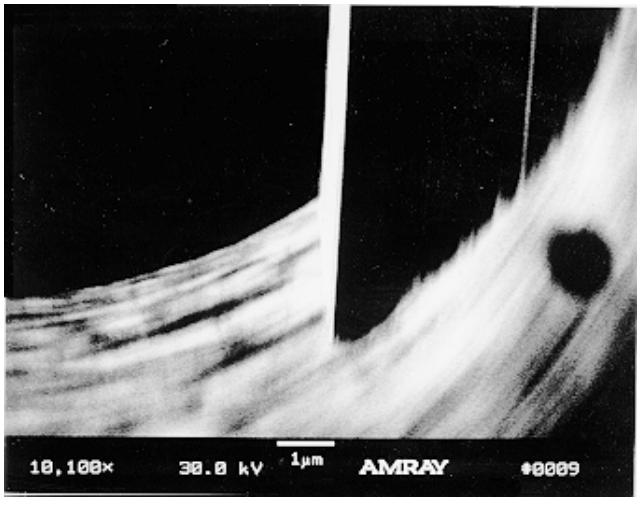

Fig. 2. An SEM micrograph of the end view of a two-faceted milling tool, made according to the technique shown in Fig. 1. The facet is the bright vertical line at the mid-point of the image. The radius of curvature of the cutting edge is of the order of 0.2 μm.

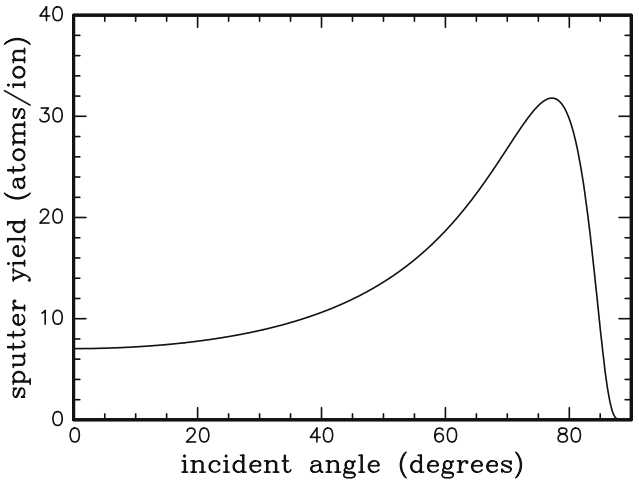

Fig. 3. The sputter yield for 20 keV Ga^+ ions on polycrystalline iron as a function of the angle of incidence. The functional form of this dependence has been experimentally verified for 30 keV Ga on Si and for 35 keV Co^+ on Si. The absolute value of the ion yield at zero angle of incidence is also known to be within 2 and 3 atoms/ion for Si.

in Fig. 3. A commercially viable FIB production process for micromilling tools would require additional ion beam control elements such as a variable spot size, a multiple tool load (or a semi-continuous tool feeding mechanism) and a semi-automated ion milling/tool rotation procedure based on pattern recognition. The spot size of the ion beam can be large in the beginning stages of cutting the facet; there is no need for high spatial resolution at this point in the process, so a large focal spot with high current can be used to remove the material efficiently. A switch to a smaller spot size is required at the final stage of the milling to ensure that the image taken clearly indicates a completely milled facet. Small features at the bottom edge of the facet can be identified in the image if the ion milling is not complete, but this requires a beam with at least 0.4 μm FWHM. Cassette designs for multiple loads have been completed (Vasile et al., 1998) and programs for automated ion milling are under development in this laboratory. Two lens FIB columns capable of producing approximately 20 nA maximum current are commercially available. The use of automated procedures and a variable spot size ion beam will reduce the tool production time from 1 h (in the manual mode) to less than 3 min.

Applications of these tools in mechanical milling of PMMA have been reported to date, and new results from a collaboration with Sandia National Laboratories (SNL) has extended the list of materials to include brass, aluminum and mild steel. (Adams et al., 1985) The total length milled in metals for a single tool now exceeds several mm, and more recent results indicate that feed rates as high as 5 cm/min can be achieved, making the practical applicability of machining processes with tools of the order of 25 μm diameter a reality. Tungsten carbide tool fabrication is also under way at SNL.

A new type of microcutting tool analogous to a shaping tool used in lathes can be made by the FIB process described above. These tools have not been reported before, and the typical pattern for an FIB milled shaping tool is shown in Fig. 4. The radius of curvature of the cutting edge in Fig. 4 is approximately one micron, and the rake angle of tools made in this way is controllable. The application of the tool in machining processes is evident from its geometry: The tool is held rigidly and the surface to be machined is moved relative to the tool, once the depth of cut has been set. The tool shown in Fig. 4 has a 30 μm maximum depth of cut, and cuts a single groove of 18 μm width. Preliminary results for this type of machining indicate a very robust process in terms of tool life. Machining parameters such as maximum feed rate, depth of cut and materials have yet to be established, but the initial results show promise for a widely applicable and practical process.

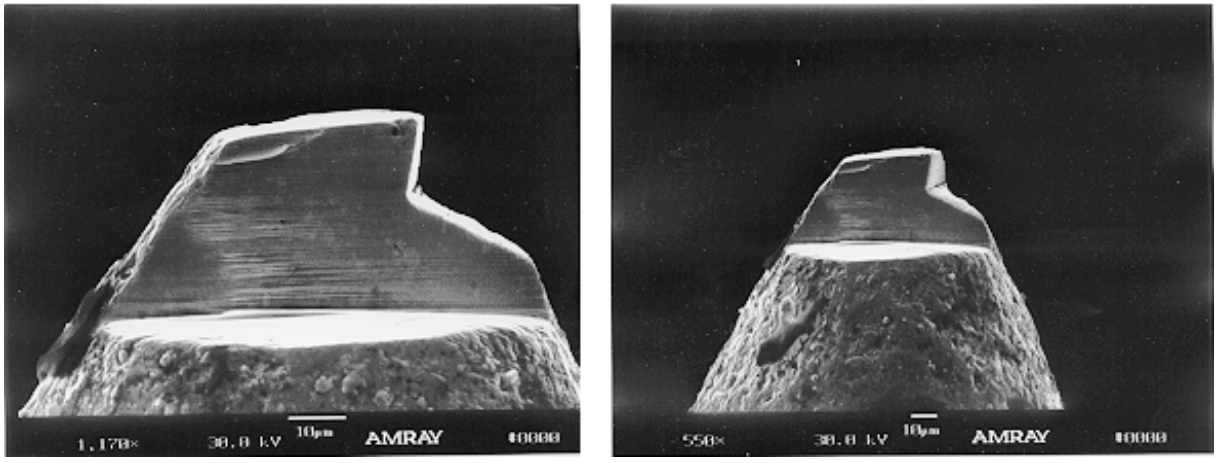

Fig. 4. SEM image of an FIB milled shaping tool. The cutting edge is at the intersection of the top surface and the right side vertical surface. The maximum depth of cut for a single channel with this tool is approximately 30 μm. The thickness of the planar slab that forms the tool has a width of 18 μm. The tool is relieved to allow release of cutting chips from the machined surface or groove. Scale bar = 10 μm.

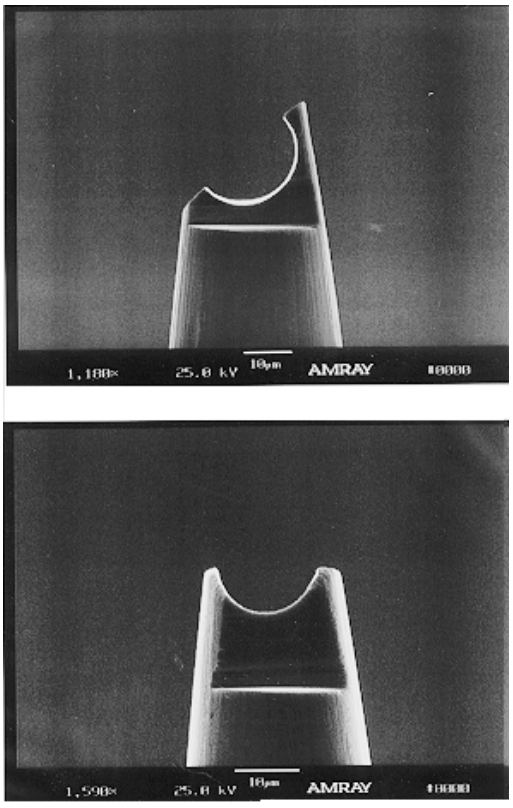

Fig. 5. A tissue stabilizer cut with the stabilization points (a) at 45° and (b) at 90° to the axis of rotation.

3. Microsurgical tools and manipulators

A variation of the milling tool fabrication process has been applied to the manufacture of specialized manipulators for microsurgical experiments involving the circulatory system. Studying the circulatory system of small test animals (mice and rats) provides a set of challenges in the micro domain. There is the need to measure the pressure in arterioles and venules, and to observe the effects of the occluding flow in these small vessels, which are typically in the range of 15–5 μm in diameter. Present practice uses glass capillaries attached to manipulators. These glass capillaries are mechanically drawn to uniform thickness by a reproducible process, but their ends lack any specialized geometry and they are also fragile. The entire procedure is done with microscopic observation, and there is a need for better tools to stabilize the tissue surrounding the test vessel and for occlusion of the vessels. A program was initiated to ion mill specialized micromanipulators in stainless steel and to adapt an existing microsurgical manipulator to accept these devices. This research was carried out in collaboration with Dr. N. Harris of the Louisiana State Medical College (Shreveport, LA).

Fabrication of the manipulators is a two part process. The first step is an anodic tapering of an inexpensive, commercially available stainless steel needle, so that the amount of ion milling required to achieve the final geometry is minimized. The anodic dissolution process is simple and very reproducible, yielding highly uniform starting geometry for all samples. The second step is ion milling using the rotational stage, with a deflection program that is adapted from the milling tool procedure shown in Fig. 1. Fig. 5 shows two view of a tissue stabilizer which is intended to limit the motion of small veins and arteries. A variety of devices based on the general concept embodied in Fig. 5 have

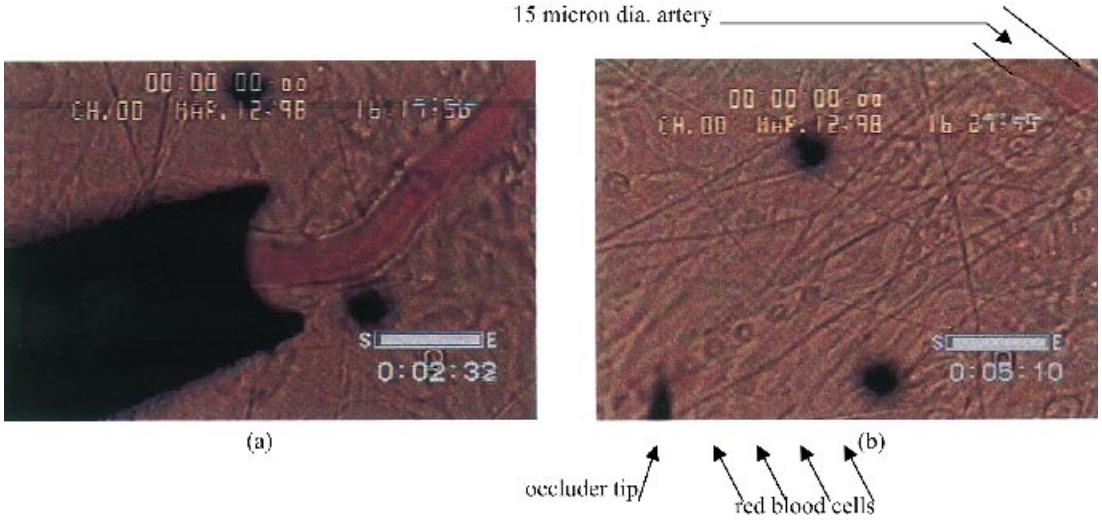

Fig. 6. Still frames from a microsurgical operation. (a) Application of the 90° stabilizer across a 15-μm diameter artery to allow insertion of a pressure measuring apparatus into the blood vessel. The moving stream of blood causes the blurred image within the vessel. (b) Occlusion of the flow of blood in a 5-μm diameter arteriole; the red blood cells are stationary, and the separation between them as a function of time is indicative of the leakage of fluid from the arteriole into the surrounding tissue. The larger 15-μm diameter artery is visible in the upper right hand corner of the image.

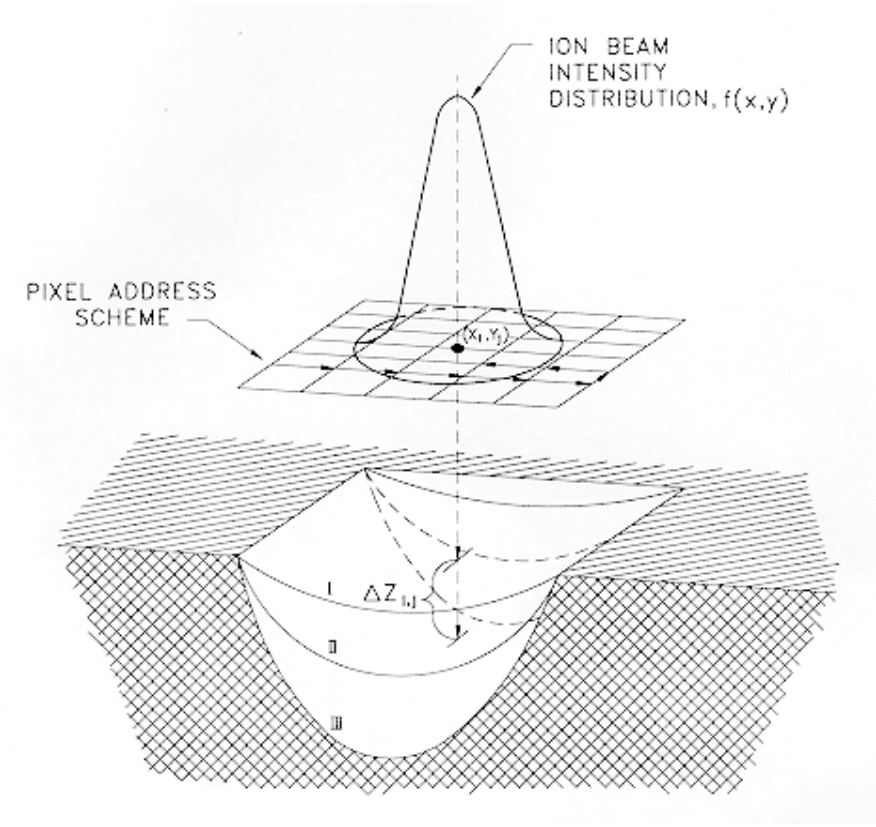

Fig. 7. The elements of the modeling technique used to generate pixel dwell times in the ion beam deflection routine to create a three-dimensional cavity. The depth increment at the point (i,j) is indicated as $\Delta Z_{i,j}$ which is the same increment solved for in Eq.(2).

been produced, and are shown in the literature (Vasile et al., 1998).

The stabilization of the tissue surrounding a 15-μm diameter arteriole with a 90° stabilizer similar to the one shown in Fig. 5 is indicated in Fig. 6(a). The tissue surrounding the arteriole must be prevented from moving so that a micropipette for the pressure measurement can be inserted in the arteriole. Fig. 6(a) is a still shot taken from a videotape of the surgical procedure as recorded by a CCD camera through a video microscopy system. The tissue surrounding the arteriole was stabilized without interfering with the blood flow through the arteriole, and the pipette was easily inserted. Occlusion of a 5-μm diameter capillary with a small FIB machined steel occluder was also accomplished during the same procedure, and the still shot showing stationary red blood cells within the capillary is shown in Fig. 6(b). The distance between the blood cells at the time of occlusion is a measure of the leakage of water through the vessel wall into the surrounding tissue, and the red blood cell adherence to the capillary wall or unrestricted flow after resumption of circulation are critical variables to observe (Harris, 1996).

The production of microsurgical manipulators of the type shown in Fig. 5 can be done rapidly and economically if a high current ion source referred to earlier is available. The spatial resolution needed can be met with a modest 0.5-μm diameter ion beam, and most of the material removal is done more efficiently with a larger, higher current beam.

A study of the production cost for microsurgical tools and micromilling tools made by the techniques described above is under way (Gray and Butler, 1998). The barriers to economical production of milling tools or microsurgical manipulators are essentially the same. A semi-automated program is needed for executing the deflection required to produce the desired shape, detect completion of the ion milling and then step to the next blank. The cost of production is also balanced by the price the market will bear. A relatively high cost may be tolerated for a highly specialized geometry in a microsurgical tool, but it is not likely that a high cost of production will be tolerated in most applications for expendable tools such as rotating milling tools.

4. Ion milling of arbitrary three-dimensional shapes

The FIB milling or sputtering of single crystal substrates can produce cavities with variations in the depth dimension, i.e. three-dimensional features with geometry based on planes of symmetry or a rotational axis of symmetry (Vasile et al., 1997). Parabolic, sinusoidal and hemispherical features were ion milled in Si (100) by a programmed dwell-time deflection scheme. Single crystal substrates are

preferred for this work as the ultimate use of the cavity will be a mold with precise dimensions and a very smooth surface finish. Grain structure of polycrystalline materials is known to limit the surface finish and the dimensional resolution (Vasile, 1993).

The technique of programming the ion beam deflection system to yield a specific geometric shape works well in principle, but it lacks absolute depth control. The reasons for the lack of depth control are in the assumptions implicit in the method: the first assumption is that the sputter yield is constant with an angle of incidence, and the second is that the ion beam intensity distribution is a constant (a delta function) and the ion beam is the same size as the pixel dimension. Neither of these situations occur; the ion beam used in this laboratory has a Gauss intensity distribution (to a first approximation) with a measured FWHM of 0.45 μm, and the pixel size in all deflection patterns is less than the ion beam FWHM. The consequence of ignoring the ion beam intensity distribution vs. the pixel size in the programmed deflection scheme is an error in the dose received by each pixel. The consequence of ignoring the change in sputter yield as the feature develops is a second additive error in the dose required to mill the feature. Neither of these factors are a source of error when milling a cavity with a rectangular cross-section, i.e. one with a constant depth, as is usually done in FIB machining.

A fundamentally different method to control the ion beam has been devised, based on a mathematical model of the combined deflection control and sputtering process (Nassar et al., 1998). The cross-section and symmetry of the final geometry are first defined. An array of pixels in the deflection pattern is then assigned to the cavity to be milled. The final cross-section of the cavity is divided into several iterations (called loops) and the ion dose needed to mill from the starting surface to the first iterative surface is calculated. The dose is calculated pixel by pixel, accounting for the contribution from adjacent pixels, and angular variation in the sputter yield is also factored into the dose calculation. An example schematic for obtaining dwell-time solutions for a parabolic cavity with a plane of symmetry is illustrated in Fig. 7.

Sputtering to the final parabolic cross-section labeled III is divided into three sub-intervals. Consider the dose needed to sputter from curve I to curve II when the ion beam is located at the deflection pixel (i, j). The dwell time at pixel (i, j) is solved for by knowing the sputter yield at the angle Θ, and by accounting for the additional dose when the ion beam is resident at adjacent pixels. The solution to this problem for all pixels in the deflection scheme takes the form of a series of linear equations:

The depth increment at the (i,j) pixel can be expressed as:

$$\Delta Z_{ij} = \sum_{k=1}^{n_1} \sum_{l=1}^{n_2} \frac{\Phi(x_k, y_l)}{\eta} f_{x_k y_l}(x_i y_j) S(\theta_{x_i y_j}) t_{kl} \Delta x_k \Delta y_l \qquad (1)$$

where $\Phi(x,y)$ is the ion flux at (x,y), η the atom density of the solid, f(x,y) the ion beam intensity distribution function, $S(\theta)$ is the angle-dependent sputter yield and $t_{k,l}$ are the dwell times. Δx and Δy are unit increments along the pixel address scheme and the summation over the indices k, l accounts for dose received at (x_i, y_j) from all pixels in the address scheme. The dwell time needed for the depth increment thus takes into account the contribution of ion flux from all pixels on the deflection plane, through the intensity distribution, $f(x,y)$. The sputter yield is also adjusted on a point-to-point basis for the change in angle of incidence as the curves I and II in Fig. 7 are traced in the deflection field. The solution for each depth increment is obtained from a matrix relationship

$$\{\Delta Z_{ij}\} = \{C_{k,l}(i,j)\}\{t_{k,l}\} \qquad (2)$$

where $C_{k,l}$ (i,j) is the local sputter relationship, $t_{k,l}$ is the dwell time and $\Delta Z_{i,j}$ is the depth increment. An array of dwell times for the ion beam on the deflection field for the first loop is thus generated, and this array is then passed on to the microprocessor that controls the deflection hardware. The mathematical model is thus a real-time solution on the FIB control computer. The depth increments in Eq.(2) are computed such that the corresponding dwell times produce sputter depths that transform curve I to curve II in Fig. 7, and so on until the final shape is reached.

Absolute yields $S(\Theta)$ at normal incidence were computed using the semi-empirical relationships of Matsunami et al. (1983) and the angular dependence of the sputter yields was calculated by the relationships given byYamaura et al. (1983). The model solutions provided by the matrix inversion routine required to solve Eq. (2) were also verified as unique solutions.

Matrices of the order N^2 by N^2 are generated for a complete solution of Eq.(2), which restricts the size of the deflection field, i.e. the number of pixels in the X and Y directions in Fig.7. Setting a limit to the overlap of the distribution function can reduce some of the computational complexity. Given a pixel dimension, D, and a value of σ for a Gauss distribution, a limit of 5σ was set for the overlap computation. If the distance between the pixel (i,j) and the pixel (k,l) is greater than 5σ, then the contribution of the Gauss function from the position (k,l) to the position (i,j) is less than 3.7×10^{-6} and treated as a zero element in the C matrix.

The accuracy of the model and the conformity of the sputtered cavity to the a-priori geometry depends upon the validity of the sputter yield, $S(\Theta)$, and the accuracy of the approximation made to the true angle of incidence as shown in Fig. 7. Fig. 3 shows that the sputter yield is zero when the angle of incidence is 90°, (grazing incidence) and a singularity results in the mathematics when this situation occurs. This is reached exactly in the model at the endpoints of a hemispherical cross-section, and it is reached approximately for parabolic cross-sections with high aspect ratios. A maximum angle of incidence was therefore set at 87°.

The SEM micrographs of a pair of independent parabolic

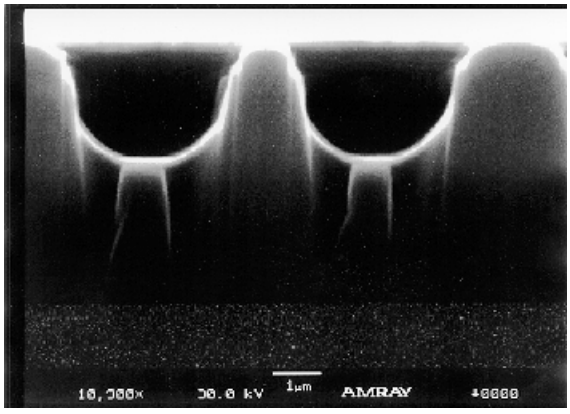

Fig. 8. Parabolic cuts ion milled in Si(100) using a 13 × 13 pixel array with 0.39 μm pixels. The depth called for in the model was 3 μm. Scale bar = 1 μm.

ion millings with a plane of symmetry are shown in Fig. 8. The solution called for in the model calculation was a parabola 3 μm deep at the deepest point on a 5 μm by 5 μm ion milling pattern in a 200-μm deflection field. A pair of features was milled as part of a repeatability test. The pixel size for the pattern is 0.39 μm (512 pixels for a 200-μm total scan) and the ion beam σ is 0.26. Three intermediate surfaces or loops were used in the calculation to get from the initial planar surface to the final parabolic surface, as indicated in Fig. 7. The pixel pattern for the ion milling procedure was only 13 × 13, which may be marginal for the kind of resolution required for microfabrication applications.

Dimensions taken from the SEM image were corrected for calibration by a single scale factor (1.17), and plotted on the equation for a parabolic cross-section in the model. These results are plotted in Fig. 9, which clearly shows very good conformity of the sputtered profile to the expected profile based on the model calculation. An error of ± 0.3 μm is estimated in the depth or *Y* dimension, and the *X* dimension must still be calibrated for the FIB.

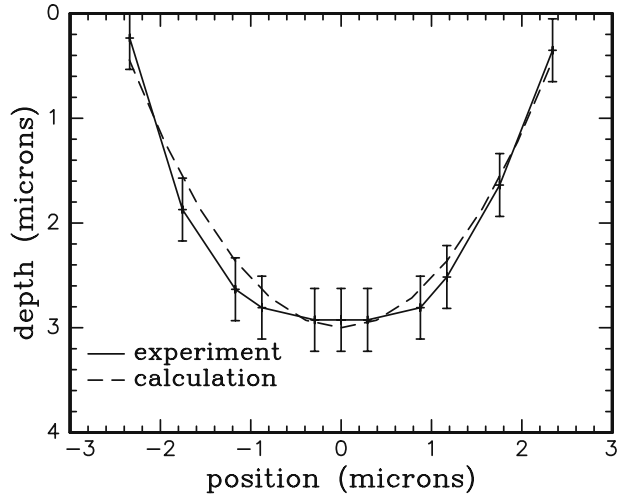

Fig. 9. Plots of the parabolic profile for one of the features ion milled in Fig. 8 plotted with the expected parabolic profile called for in the model calculation. A single scale factor (1.17) was applied to the *X* and *Y*-axes to account for the calibration discrepancy between the FIB and the SEM.

Departures in the ion milled features from the model solution occur in two places. There is a small length along the bottom of the parabolic feature that is flat, from the midpoint (the origin on Fig. 9) to about 0.5 μm in either the positive or negative direction, and there are sharp-cornered features at the shallow ends of the parabola. The flat segment maybe due to some re-deposited material and the lack of resolution in the calculation may also account for both of these departures. Vertical striations on the sidewall of the Si substrate are an artifact of the ion milling procedure used to section the feature. Milling features with loop values ranging to ten did not improve the resolution of the feature or the conformity to the model. Similar agreement was obtained with parabolic milling of 5 μm deep features, using the same deflection parameters.

A cosine cross-section with two periods over 7.5 μm and a depth of 3 μm was solved for and ion milled in Si(100). The result of this milling is shown in Fig. 10(a). The cross-section of the feature appears to be segmented rather than a smooth curve, and this is consistent with the relationship of the pixel size and the ion beam (0.49 μm pixel dimension and 0.45 μm FWHM ion beam). The ion milling removed excess material at the maximum in the cosine function, which indicates an error in the solution for the overlap contribution in this region. Fig. 10(b) shows the profile of the expected cosine curve from the model solution plotted with the experimental points taken from Fig. 10(a). Error bars are omitted in Fig. 10(b) for the sake of clarity, but they are the same size as those in Fig. 9. The general shape of the model calculation is obtained, and there is agreement between the ion milled depth and the model.

A comparison between the dwell-time array (the *t* matrix in Eq. (2)) and the shape of the ion milled feature or the desired cross-section in the model is instructive. The display of dwell-time solutions for a series of pixels for the feature cross-section will not reflect the geometry of the feature when the overlap or the angle correction is significant. Fig. 11 shows such a plot for the dwell times corresponding to the ion milling shown in Fig.10, for five loops or surfaces. The largest corrections correspond to the side walls of the feature, where the angle of incidence is large and the sputter yield is high. The correction also becomes more significant as the required feature depth increases.

The results embodied in Figs. 8–11 show that the solutions of the model calculation actually control the ion beam deflection to produce cavities that replicate the desired geometry to a reasonable degree. The agreement in depth is probably as good as can be expected in view of the accuracy to which the sputter yield is known. The ion beam current must be constant over the entire sputtering process as well. A larger deflection field will most likely improve the resolution of the feature surface, i.e., the smoothness of the contours obtained. A method for factoring the *C* matrix

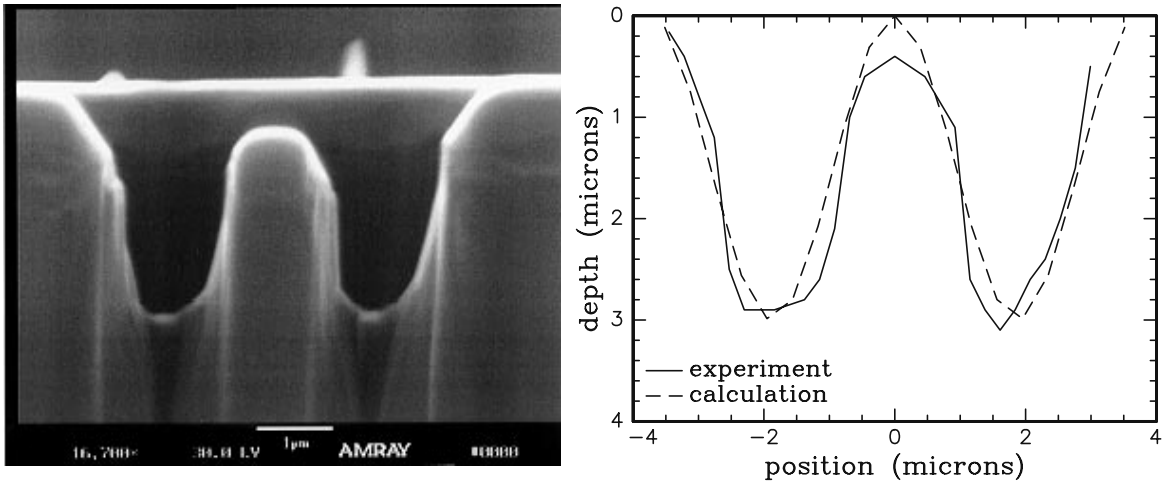

(a) **(b)**

Fig. 10. The results of milling a 3-μm deep cosine function with a plane of symmetry. (a) The profile of the cosine function in Si(100) from a 13 × 13 pixel array, using 0.49 μm pixels. (b) An overlay of the expected model profile (dashed line) with the experimental profile (solid line) taken from (a). Error bars have been omitted for clarity.

has been worked out which reduces the computation from an $N^2 \times N^2$ matrix to an $N \times N$ matrix, thus allowing very much larger deflection fields and smaller pixel sizes. Solutions from the factored matrix were determined to be identical to those previously obtained and there are pending experimental tests. The mathematical model developed in this study does not treat redeposition of sputtered material, which will alter the geometry of any high aspect ratio features, relative to the geometry called for in the model.

5. Summary

This article has treated focused ion beam applications that are essentially non-diagnostic, and potentially capable of producing microstructures. The route to production may be a direct one as in the application to microsurgical manipulators, or it may be an indirect one as in the production of micromilling tools. In both of these examples, the commercial application will depend on the development of automated sequences for pattern recognition, stage positioning and end point decisions. Ion milling time can reach acceptable limits with the use of a high current column. The ion milling of three-dimensional features with close dimensional control can be achieved for parabolas and for cosine functions with a plane of symmetry. Other symmetries have been coded but not tested yet. Further efforts are needed to improve the contours or surface finish obtained in this method and then the myriad of symmetries available will be ion milled. The final step to mass replication will also require development, but this is not envisioned as a major obstacle.

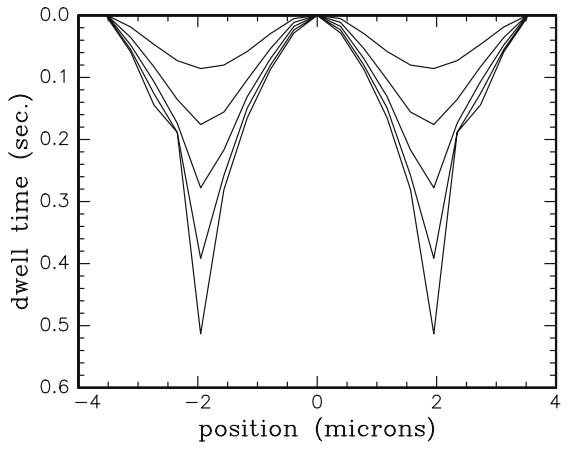

Fig. 11. A plot of the dwell times for the cosine milling in Fig. 10. The dwell-time profile is plotted for each of the surfaces (loops) used in the calculation to arrive at the final surface.

Acknowledgements

The authors would like to acknowledge G.L. Benavides, D.P. Adams and the staff of the Advanced Manufacturing Processes Laboratory of Sandia National Laboratories for their contribution to this work, the National Science Foundation for partial support under grant #ECS9503204, the Louisiana Board of Regents, and the Institute for Micromanufacturing for their support. The contributions of Dr. N. Harriott, Bell Labs, Lucent Technologies are also deeply appreciated.

References

Adams, D., Benavides, G., Vasile, M., 1998, Micrometer-scale machining of metals and polymers enabled by focused ion beam techniques. Symposium AA, Materials Science of Microelectromechanical Systems (MEMS) Devices, Materials Research Society Meeting, Boston, MA, Dec 1–2.

Bell, A., Swanson, L., 1985. Mechanisms of liquid metal ion source operation. Nucl. Instrum. Meth. B10/11, 783–787.

Blauner, P., Mauer, J., 1993. X-ray mask repair. IBM J. Res. Dev. 37, 421.

Crell, C., Friedrich, S., Schreiber, H.U., Weick, A., 1997. J. Appl Phys. 82, 4616.

Friedrich, C., Vasile, M., 1996. Development of the micromilling process for high aspect ratio microstructures. J. Microelectromech. Sys. 5, 33.

Friedrich, C., Coane, P., Vasile, M., 1997. Micromilling development and applications for microfabrication. Microelectron. Engng 35, 367.

Gamo, K., 1991. Focused ion beam technology. Vacuum 42, 89.

Gray, A., Butler, A., 1998 Personal communication.

Gross, M., Harriott, L., Opila, R., 1990. J. Appl. Phys. 68, 4820.

Harris, N., 1996. Mechanisms underlying enhanced capillary filtration induced by platelet activating factor. Am. J. Physiol. 270H, 127.

Harriott, L., 1987. A second generation focused ion beam micromachining system. Proc. SPIE 773, 190.

Ishitani, T., Ohnishi, T., Kawanami, Y., 1990. Micromachining and device transplantation using focused ion beams. Jpn. J. Appl. Phys. 29, 2283.

Ishitani, T., Taniguchi, Y., Isakozawa, S., Yaguchi, T., Matsumoto, H., Kamino, T., 1998. Proposals for exact-point transmission-electron microscopy using focused ion beam sample-preparation techniques. J. Vac. Sci. Technol. B16, 2532.

Itoh, F., Shimase, A., Satoshi, H., 1990. Two-dimensional profile simulation of focused ion beam milling of LSI. J. Electrochem. Soc. 137, 983.

Kalburge, A., Konkar, A., Ramachandran, T., Chen, P., Madhukar, A., 1997. Focused ion beam assisted chemically etched mesas on GaAs(001) and the nature of subsequent molecular beam epitaxial growth. J. Appl. Phys. 82, 859.

Konig, H., Mais, N., Hofling, E., Reithmaier, J., Forchel, A., Mussig, H., Brugger, H., 1998. Focused ion beam implantation for opto- and microelectronic devices. J. Vac. Sci. Technol. B16, 2562.

Musil, C., Melngailis, J., Etchin, S., Hayes, T., 1996. Dose rate effects in GaAs investigated by discrete pulsed implantation using a focused ion beam. J. Appl. Phys. 80, 3727.

Matsunami, N., Yamamura, Y., Itakawa, Y., Itoh, N., Kazumata, S., Miyagawa, K. Morita, K., Shimizu, S.,1983, Energy dependence of sputtering yields of monatomic solids. Report IPPJ-AM-14, Institute of Plasma Physics, Nagoya University, Nagoya, Japan.

Nagamchi, S., Ueda, M., Sakakima, H., Satomi, M., Ishikawa, J., 1996. Giant magnetoresistance in Co/Cu multilayers fabricated by focused ion beam direct deposition. J. Appl. Phys. 80, 4217.

Nikawa, K., 1991. Application of focused ion beam techniques to failure analysis of very large scale integrations. J. Vac. Sci. Technol., B 9, 2566.

Nassar, R., Vasile, M., Zhang, W., 1998. Mathematical modelling of focused ion beam microfabrication. J. Vac. Sci. Technol. B16, 109.

Orloff, J., 1993. High resolution focused ion beams. Rev. Sci. Instrum. 64, 1105.

Saka, H., 1998. Transmission electron microscopy observation of thin foil specimens prepared by means of a focused ion beam. J. Vac. Sci. Technol. B16, 2522.

Vasile, M., Harriott, L., 1989. Focused ion beam stimulated deposition of organic compounds. J. Vac. Sci. Technol., B7.

Vasile, M., Grigg, D., Griffith, J., Fitzgerald, E., Russell, P., 1991. Scanning probe tips formed by focused ion beams. Rev. Sci. Instrum. 62, 2167.

Vasile, M., Schwalm, S., Biddick, C., 1993, Microfabrication by ion milling: the lathe technique. In: Pisano, A.P., Jara-Almonte, J., Trimmer, W. (Eds.), Proceedings of the ASME, DSC, Vol. 46, Micromechanical Systems, Book no. H00832-1993. pp 81.

Vasile, M., Biddick, C., Schwalm, S., 1994. Microfabrication by ion milling: the lathe technique. J. Vac. Sci. Technol. B12, 2388.

Vasile, M., Friedrich, C., Kikkeri, B., McElhannon, R., 1996. Micrometer scale machining: tool fabrication and initial results. Precision Engng 19, 180.

Vasile, M., Niu, Z., Nassar, R., Zhang, W., Liu, S., 1997. Focused ion beam milling: depth control for three-dimensional microfabrication. J. Vac. Sci. Techol. B15, 2350.

Vasile, M., Nassar, R., Xie, J., 1998. Focused ion beam technology applied to microstructure fabrication. J. Vac. Sci. Technol. B16, 2499.

Ximen, H., DeFreez, R., Orloff, J., Elliott, R., Evans, G., Carlson, N., Lurie, M., Bour, D., 1990. Focused ion beam micromached three-dimensional features by means of a digital scan. J. Vac. Sci. Technol. B8, 1361.

Yamaura, Y., Itakawa, Y., Itoh, N., 1983, Angular dependence of sputter yields of monatomic solids. Report IPPJ-AM-26, Institute of Plasma Physics, Nagoya University, Nagoya, Japan.

Young, R., 1993. Micro-machining using a focused ion beam. Vacuum 44, 353.